Supporting Information

Value-Added Upcycling of Spent Low-Nickel into High-Nickel Layered Oxide Cathode via Eutectic Salt System

*Mengyuan Li,[a] Di Shao,[a] Zhihao Mao,[a] Zengjie Fan,[a] Lei Xu,[a] Hui Dou,[a] Zuling Peng,[*b] Bing Ding[*a, c] and Xiaogang Zhang[*a, c]*

[a] Jiangsu Key Laboratory of Electrochemical Energy-Storage Technologies, College of Materials Science and Technology, Nanjing University of Aeronautics and Astronautics, Nanjing 210016, China.

E-mail: bingding@nuaa.edu.cn

[b] CALB Group Ltd, Changzhou 213222, China

E-mail: zuling.peng@calb-tech.com

[c] State Key Laboratory of Mechanics and Control for Aerospace Structures, Nanjing University of Aeronautics and Astronautics, No. 29 Yudao Street, Nanjing 210016, China.

Experimental section

Materials and preparation

Two degraded experimental modules (provided by CALB) were discharged, manually disassembled, and manually separated into cathode, anode electrode material, and separator. The obtained cathode underwent detachment, crushing, and impurity removal processes to obtain ternary cathode powder (D-NCM5).

C-NCM7, and graphite negative electrode material (provided by figure S1 CALB, with doping and coating) were used. $LiOH{\cdot}H_2O$ (battery-grade $LiOH{\cdot}H_2O$ provided by Sichuan Zhiyuan Lithium), Li_2CO_3 (MCKLIN AR, 99.5%), $LiNO_3$ (MCKLIN AR, 99%), LiI (MCKLIN AR, 99%), Li_2SO_4 (MCKLIN AR, 99%), CH_3COOLi (MCKLIN AR, 99%), $NiCO_3$ (MCKLIN AR, 98%), $MnCO_3$ (MCKLIN AR), Ni_2O_3 (MCKLIN AR, 99%), and MnO (MCKLIN AR, 99%) were used.

D-NCM5 was mixed with $NiCO_3$, $MnCO_3$, LiOH, and Li_2CO_3 in a molar ratio of 0.85:0.09:1:0.2. The mixture was dried at 120 °C for 6 h to remove residual moisture. Subsequently, the mixture was ball-milled for 8 h to ensure a uniform dispersion of the material. The resulting mixture was then placed in an alumina crucible and transferred to a tubular

furnace. The mixture was then heated under oxygen gas at 500 °C and then at 950 °C for 6 and 11 h, respectively. After cooling down to room temperature, the obtained material was washed with a water to remove residual lithium ions on the surface, followed by drying at 120 °C for 6 h. Finally, the material was calcined at 750 °C for 5 h, with a heating rate of 5 °C min^{-1}, resulting in the formation of RC-NCM7. RO-NCM7 is prepared similarly to RC-NCM7.

Material characterizations

Scanning electron microscopy (SEM, Gemini SEM 300), focused ion/electron beam dual-beam system (FIB, SCIOS 2HiVac), and transmission electron microscopy (TEM, JEM 2100) were employed to investigated the morphologies. X-ray diffraction (XRD, Rigaku Ultima IV) analysis was performed using Cu Kα radiation, with a scanning rate of 1 ° min^{-1}. Inductively coupled plasma emission spectroscopy (iCAP PRO X DUO) and X-ray photoelectron spectroscopy (XPS, Thermo Scientific K-Alpha$^+$) was used to investigate the chemical compositions of different materials. The thermal gravimetric curves and differential thermal gravimetric curves (TG-DTG, STA 449 F5 Jupiter) of LiOH and $LiNO_3$, LiOH and Li_2CO_3, and RO-NCM7 and RC-NCM7 mixtures were obtained in the temperature range of 10 to 600°C (heating rate: 10 °C min^{-1}).

Battery assembly and testing

The cathode RC-NCM7 (RO-NCM7), Super P conductive agent, and PVDF (94:3:3) were mixed in a slurry tank for slurry preparation. The resulting slurry is then coated onto a current collector using a coating machine. Subsequently, the coated electrode was placed in a vacuum oven at 120°C for 12 h for drying. After drying, the electrode material was cut into strips of 8 cm width and then subjected to calorimetry at a pressure of 10 MPa using a roll press. Finally, the finished electrodes are obtained. The electrode was further cut into circular discs with a diameter of Φ12 cm for assembly into both a half-cell with metallic lithium as the negative electrode and a CR2016 button cell with graphite as the negative electrode. The mass loading of active material is 10 mg cm^{-2}, and the N/P of the full battery is about 1.1. The electrolyte used was a mixture of 1 M $LiPF_6$, ethylene carbonate (EC), dimethyl carbonate (DMC), and diethyl carbonate (DEC) in equal volumes.

For electrochemical characterization, the assembled cells were tested using a Neware battery test system. The cells were initially activated by performing two activation cycles between 3 V and 4.4 V vs. Li/Li$^+$. After activation, a constant current charge-discharge test, a rate performance test, and a cycling test were performed in a voltage range of 3 V to 4.4 V. The rate performance tests were carried out at current densities ranging from 0.1C to 10C (1C = 170

mAh g^{-1}). The galvanized intermittent titration technique (GITT) tests involved two activation cycles at 0.1C, followed by a 10-minute constant current charge, a 30-minute rest, and a subsequent constant current discharge for ten minutes, with a 30-minute rest period between cycles. Electrochemical properties were evaluated using a Princeton Applied Research Workstation with a potential scan range of 3.0 V to 4.4 V and a scan rate of 0.1 mV s^{-1}. Electrochemical impedance spectroscopy (EIS) tests were conducted using a Gamry electrochemical workstation with the cells in an as-prepared, non-activated state.

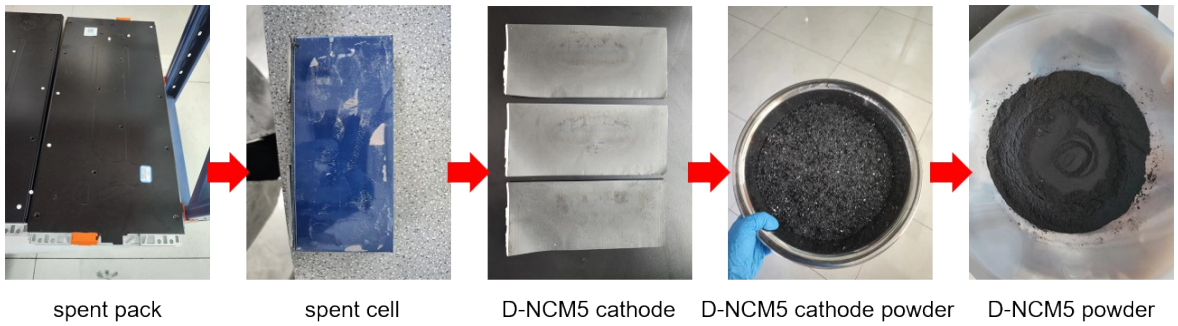

Figure S1. The process of obtain spent D-NCM5 powder from degraded LIB pack.

Note: The NCM5 module sourced from the market was retired and subsequently subjected to discharging and disassembly, resulting in individual cells. These cells were further dismantled to extract the spent cathode. The electrode sheets undergo crushing and detachment procedures to yield the spent cathode powder. Lastly, a purification process is applied to obtain D-NCM5.

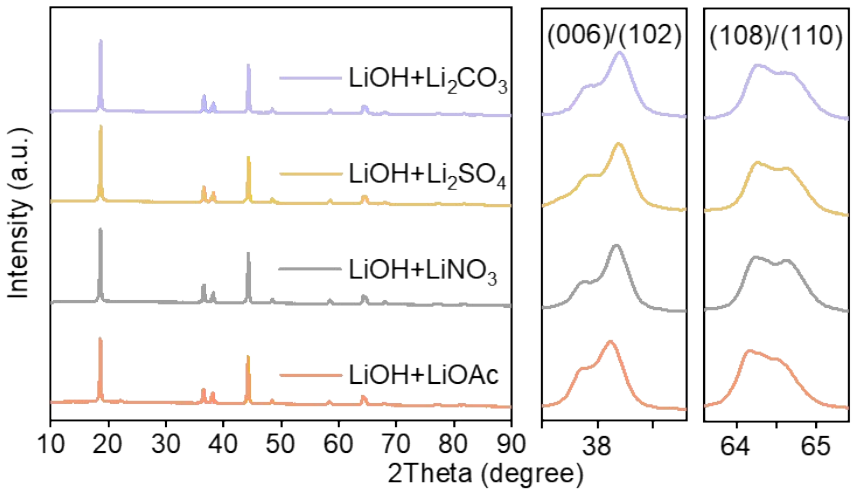

Figure S2. XRD patterns of the upcycled NCM7 materials prepared using different eutectic molten salt systems.

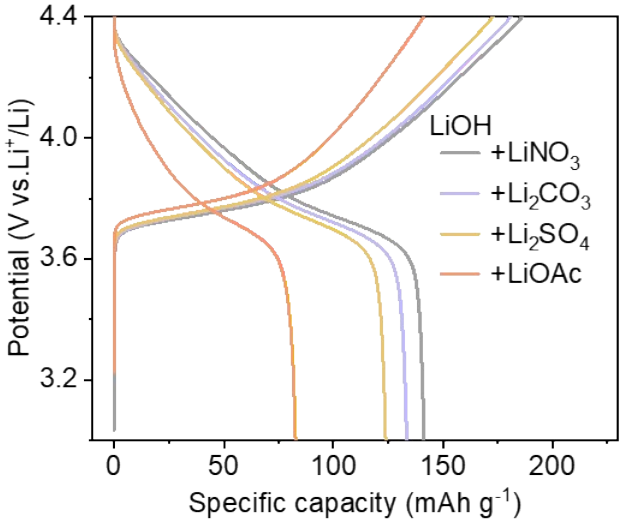

Figure S3. Initial charge/discharge curves of the NCM7 cathodes prepared using different eutectic molten salt system.

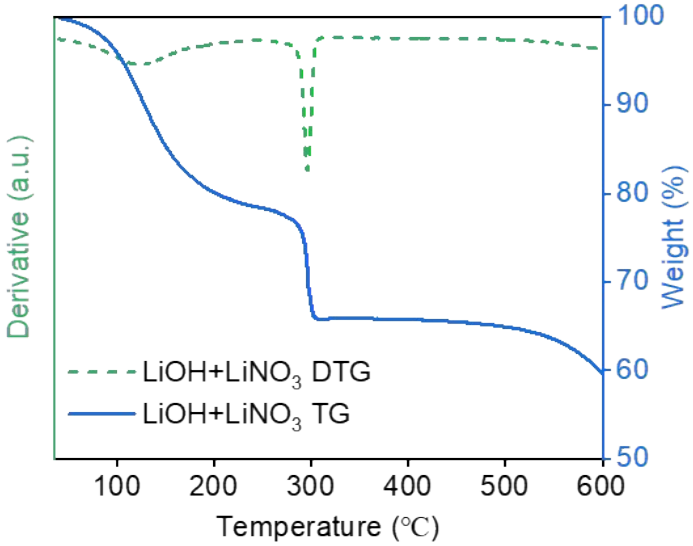

Figure S4. TG curve of LiOH-$LiNO_3$ eutectic salt.

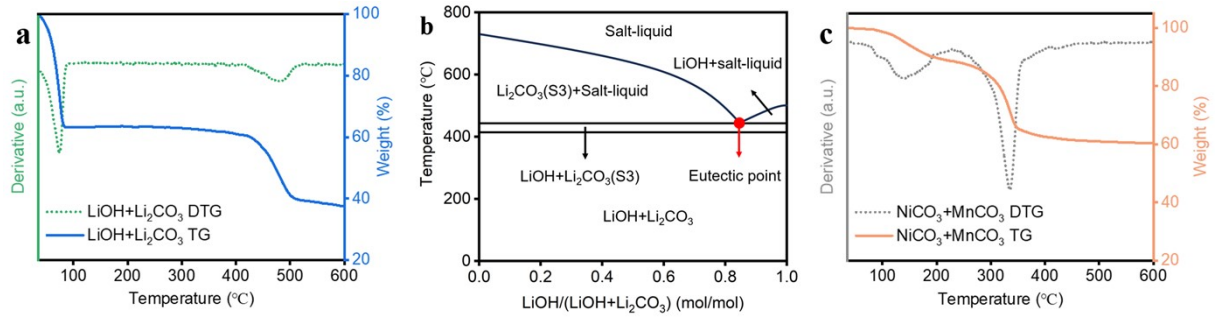

Figure S5. (a) TG curve of LiOH-Li_2CO_3 eutectic salt, (b) Phase diagram of LiOH-Li_2CO_3, (c) TG curve of $NiCO_3$ and $MnCO_3$.

Note: The temperature range of 0-100 ºC in the TG curve corresponds to a dehydration process resulting from the moisture absorption by LiOH and Li_2CO_3 from the surrounding air. Within the 420-500 ºC range, the mixture undergoes a transition from a solid state to a liquid state, with a reaction peak identified at 477 ºC. According to the phase diagram, the eutectic point of LiOH-Li_2CO_3 salt is approximately 430 ºC.

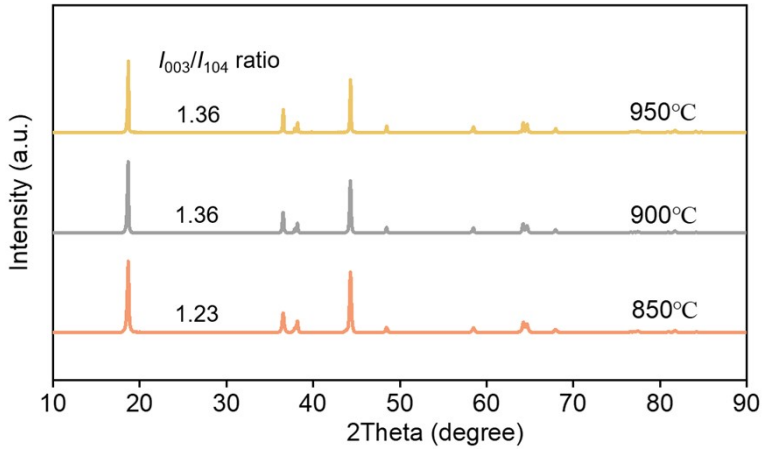

Figure S6. XRD patterns of the NCM7 materials prepared at different temperatures.

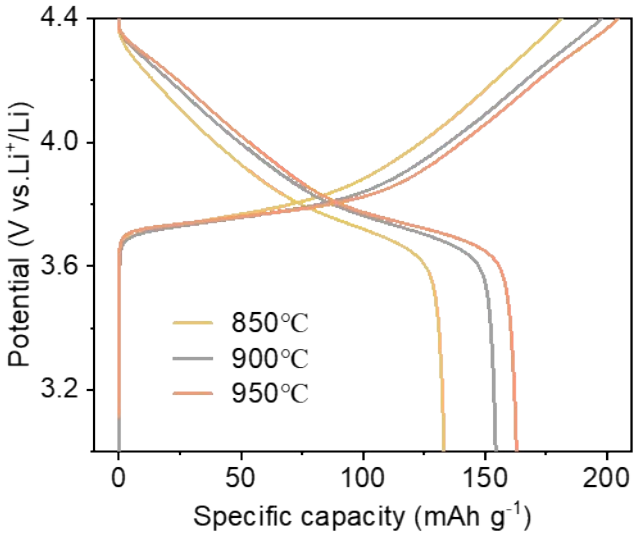

Figure S7. Initial charge/discharge profiles of NCM7 cathodes prepared at different temperatures.

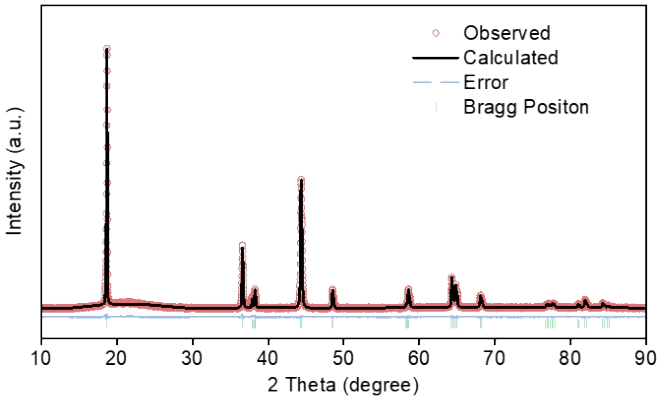

Figure S8. Refined XRD patterns of RO-NCM7.

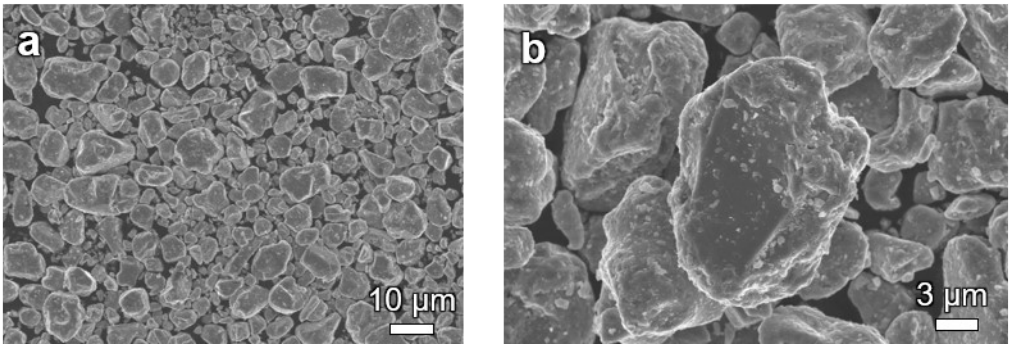

Figure S9. SEM images of RO-NCM7.

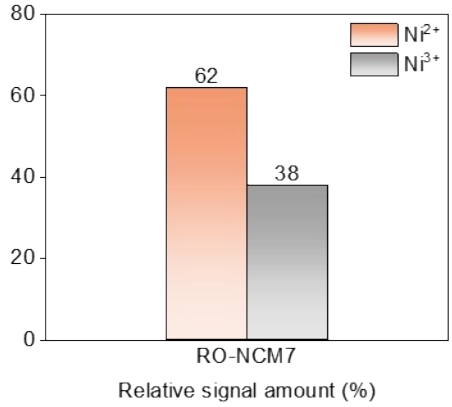

Figure S10. Ni content ratio.

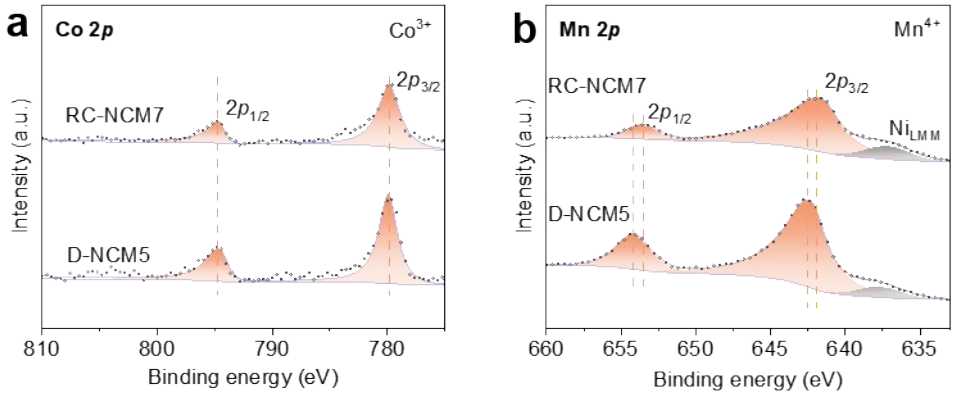

Figure S11. (a) Co$2p_{3/2}$ XPS spectra, (b) Mn$2p_{3/2}$ XPS spectra.

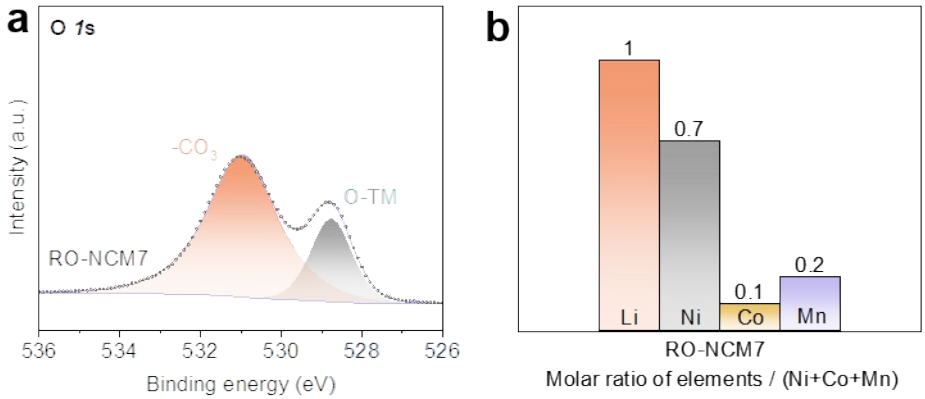

Figure S12. (a) XPS O*1s* spectra, and (b) ICP result of RO-NCM7.

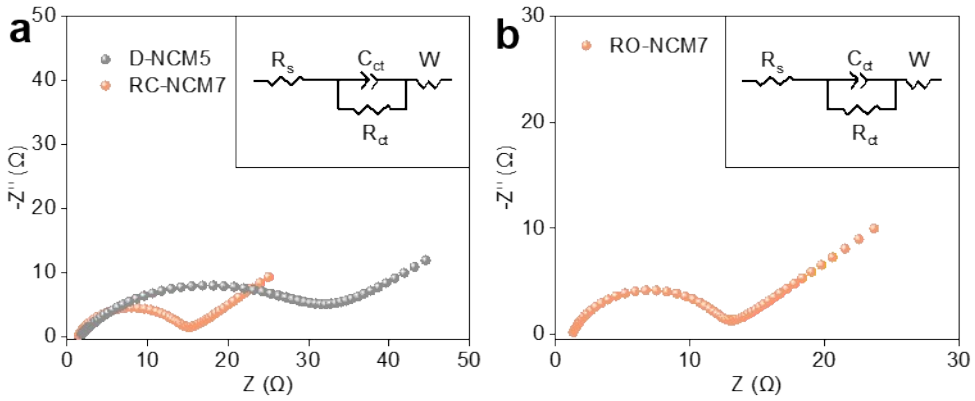

Figure S13. Nyquist plots before cycling: (a) D-NCM5 and RC-NCM7, (b) RO-NCM7.

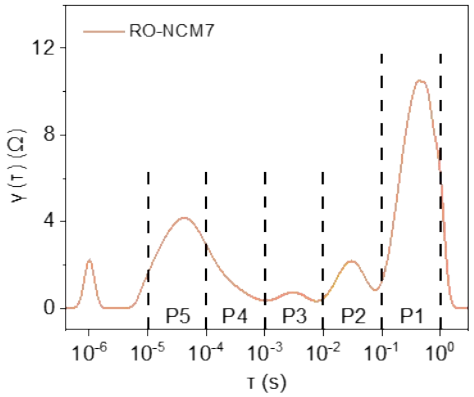

Figure S14. DRT analyzed within Nyquist plot: RO-NCM7.

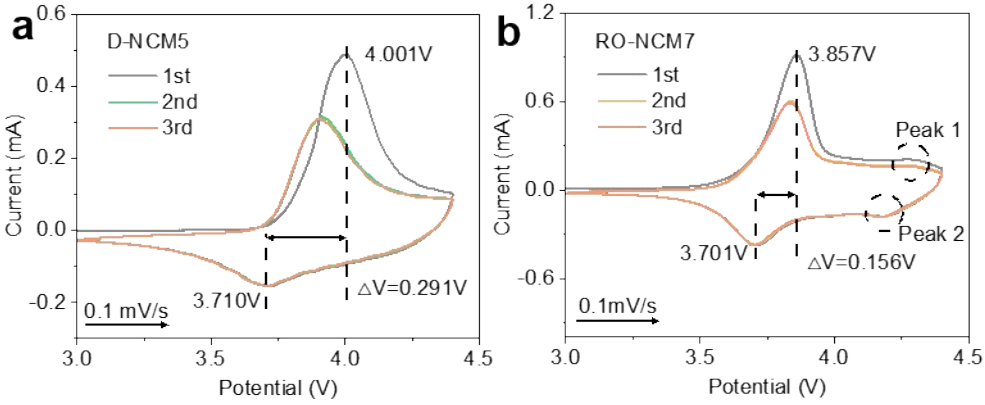

Figure S15. CV curves of initial three cycles: (a) D-NCM5 (b) RO-NCM7.

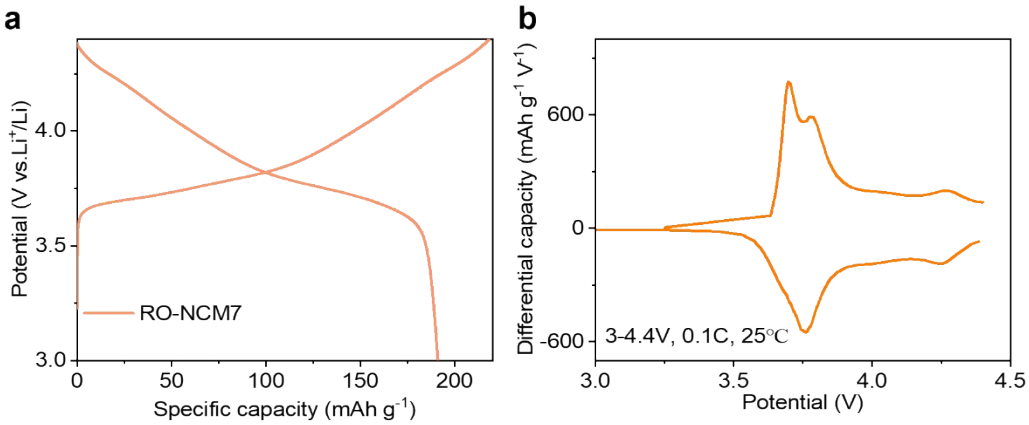

Figure S16. (a) Initial charge/discharge profile and (b) differential capacity curve of RO-NCM7 cathode.

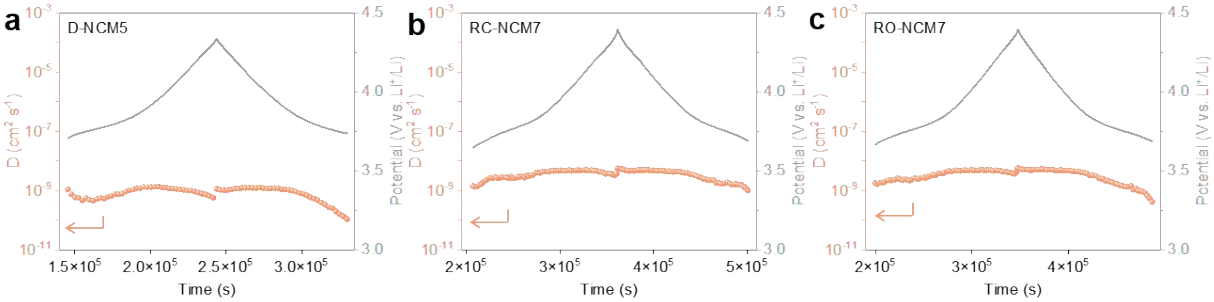

Figure S17. Lithium-ion transport rate of (a) D-NCM5, (b) RC-NCM7 and (c) RO-NCM7.

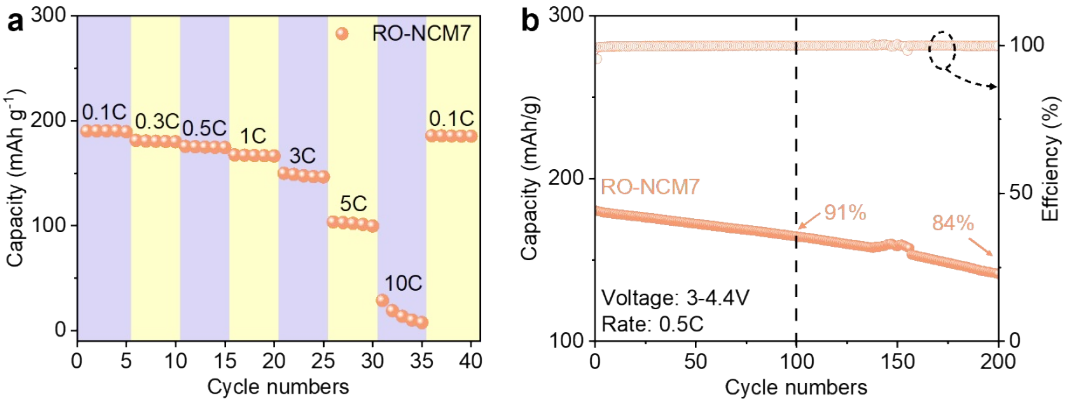

Figure S18. (a) Rate performance and (b) cycling performance at 0.5C of RO-NCM7 cathode.

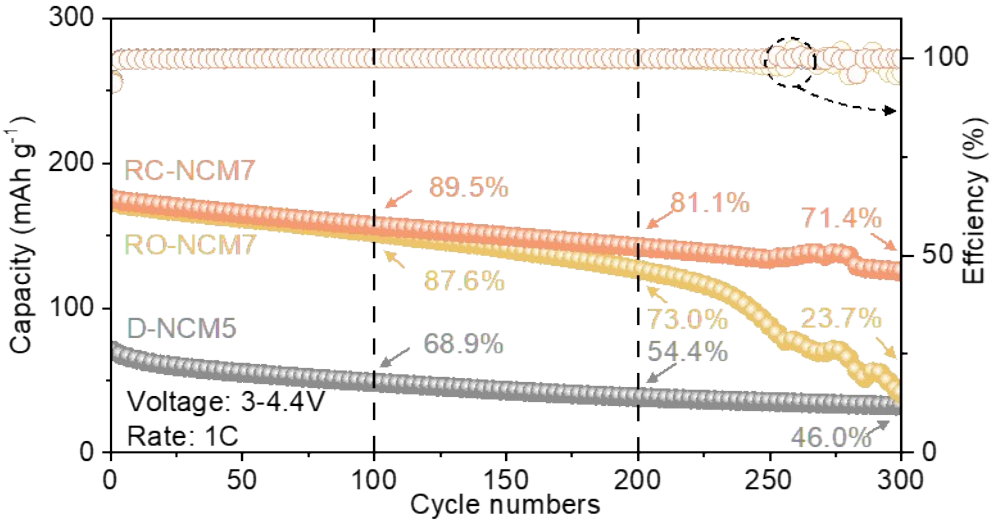

Figure S19. Cycling performances of three cathodes at 1C.

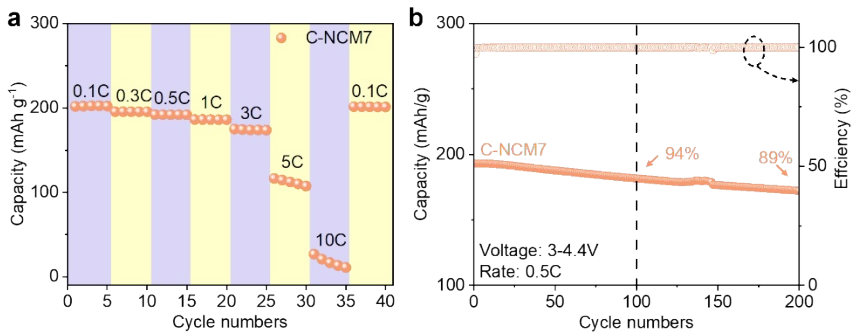

Figure S20. (a) Rate performance and (b) cycling performance at 0.5C of C-NCM7 cathode.

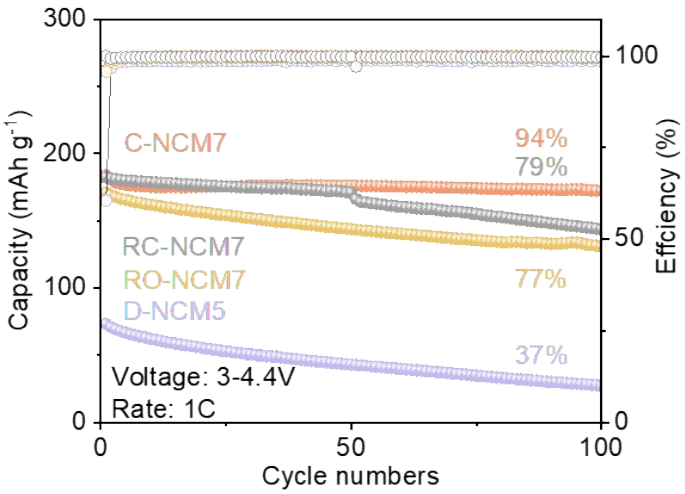

Figure S21. Cycling performances of full cells with different cathodes.

Table S1 Lattice parameters of RC-NCM7, RO-NCM7, D-NCM5

Material	**c/Å**	**V/Å^3**	**c/a**	I_{003}/I_{104}	**Li/Ni Antisite Ratio**	R_p	R_{wp}
RC-NCM7	14.2632	102.49	4.952	2.00	5.1%	0.69%	1.49%
RO-NCM7	14.2461	102.13	4.951	1.76	7.1%	2.04%	2.67%
D-NCM5	14.3029	103.39	4.950	1.18	12.2%	0.89%	1.69%

Table S2. Electrochemical performance compassions of regenerated NCM523 using molten salt method with different additives.

Materials	**Additives**	**Discharge capacity (mAh g^{-1})**	**Capacity after 100 cycles**	**Capacity Retention (%)**	**Reference**
NCM523	LiOH + $LiNO_3$	165 (0.1 C)	130 (1 C)	89	S1
	LiOH + Li_2CO_3	160 (0.1 C)	136 (1 C)	93	S2
	LiOH + $LiNO_3$ + Li_2CO_3	157 (0.1 C)	142 (1 C)	85	S3
	LiOH + $LiNO_3$+ CH_3COOLi	166 (0.1 C)	150 (0.5 C)	94	S4
	LiOH + LiI	150 (0.1 C)	125 (0.5 C)	89	S5
	LiOH + $LiNO_3$ +LSA	167 (0.1 C)	155 (0.5 C)	96	S6
	$LiNO_3$	160 (0.1 C)	152 (0.2 C)	96	S7
	Li_2CO_3	180 (0.2 C)	147 (1 C)	88	S8
	LiOH + CH_3COOLi	158 (0.2 C)	124 (1 C)	85	S9
	LiOH + Li_2CO_3+ $NiCO_3$+$MnCO_3$	191 (0.1 C)	164 (1 C)	91	This work

Table S3. Cost per kg cell recycled in China ($).[S10, S11]

Method	LCO	NCM111	NCM811	LFP
Pyrometallurgical process	4.18	2.38	2.18	0.18
Hydrometallurgical process	3.75	1.95	1.75	0.25
Direct recycling process	4.13	2.33	2.13	0.13

Table S4. Revenue generated per kg cell recycled ($).[S10, S11]

Method	LCO	NCM111	NCM811	LFP
Pyrometallurgical process	11.66	5.26	3.54	0.83
Hydrometallurgical process	11.8	5.61	3.74	0.96
Direct recycling process	17.01	7.33	5.57	5.09

References:

S1 Y. Shi, M. Zhang, Y. S. Meng and Z. Chen, *Adv. Energy Mater.*, 2019, **9**, 1900454.

S2 G. Jiang, Y. Zhang, Q. Meng, Y. Zhang, P. Dong, M. Zhang and X. Yang, *ACS Sust. Chem. Eng.*, 2020, **8**, 18138-18147.

S3 Z. Xiao, Y. Yang, Y. Li, X. He, J. Shen, L. Ye, F. Yu, B. Zhang and X. Ou, *Small*, 2024, **20**, 2309685.

S4 Z. Qin, Z. Wen, Y. Xu, Z. Zheng, M. Bai, N. Zhang, C. Jia, H. B. Wu and G. Chen, *Small*, 2022, **18**, 2106719.

S5 J. Ma, J. Wang, K. Jia, Z. Liang, G. Ji, Z. Zhuang, G. Zhou and H.-M. Cheng, *J. Am. Chem. Soc.*, 2022, **144**, 20306-20314.

S6 X. Liu, R. Wang, S. Liu, J. Pu, H. Xie, M. Wu, D. Liu, Y. Li and J. Liu, *Adv. Energy Mater.*, 2023, **13**, 2302987.

S7 B. Deng, Z. Zhou, W. Wang and D. Wang, *ACS Sustain. Chem. Eng.*, 2020, **8**, 14022-14029.

S8 H. Dong, H. Wang, J. Qi, J. Wang, W. Ji, J. Pan, X. Li, Y. Yin and S. Yang, *ACS Sust. Chem. Eng.*, 2022, **10**, 11587-11596.

S9 B. Liu, J. Huang, J. Song, K. Liao, J. Si, B. Wen, M. Zhou, Y. Cheng, J. Gao and Y. Xia, *Energy & Fuels*, 2022, **36**, 6552-6559.

S10 Y. Yang, E. G. Okonkwo, G. Huang, S. Xu, W. Sun and Y. He, *Energy Storage Mater.*, 2021, **36**, 186-212.

S11 R. Sommerville, P. C. Zhu, M. A. Rajaeifar, O. Heidrich, V. Goodship and E. Kendrick,

Resour. Conserv. Recy., 2021, **165**, 105219.